

Magnesium isotope ratios in Hyades stars¹

David Yong, David L. Lambert, Carlos Allende Prieto

Department of Astronomy, University of Texas, Austin, TX 78712

tofu,dll,callende@astro.as.utexas.edu

and

Diane B. Paulson

*Department of Astronomy, University of Michigan, 830 Dennison Building, Ann Arbor, MI
48109*

apodis@umich.edu

ABSTRACT

Using classical model atmospheres and an LTE analysis, Mg isotope ratios $^{24}\text{Mg}:$ $^{25}\text{Mg}:$ ^{26}Mg are measured in 32 Hyades dwarfs covering $4000\text{K} \leq T_{\text{eff}} \leq 5000\text{K}$. We find no significant trend in any isotope ratio versus T_{eff} and the mean isotope ratio is in excellent agreement with the solar value. We determine stellar parameters and Fe abundances for 56 Hyades dwarfs covering $4000\text{K} \leq T_{\text{eff}} \leq 6200\text{K}$. For stars warmer than 4700K, we derive a cluster mean value of $[\text{Fe}/\text{H}] = 0.16 \pm 0.02$ ($\sigma = 0.1$), in good agreement with previous studies. For stars cooler than 4700K, we find that the abundance of Fe from ionized lines exceeds the abundance of Fe from neutral lines. At 4700K $[\text{Fe}/\text{H}]_{\text{II}} - [\text{Fe}/\text{H}]_{\text{I}} \simeq 0.3$ dex while at 4000K $[\text{Fe}/\text{H}]_{\text{II}} - [\text{Fe}/\text{H}]_{\text{I}} \simeq 1.2$ dex. This discrepancy between the Fe abundance from neutral and ionized lines likely reflects inadequacies in the model atmospheres and the presence of Non-LTE or other effects. Despite the inability of the models to reproduce ionization equilibrium for Fe, the Mg isotope ratios appear immune to these problems and remain a powerful tool for studying Galactic chemical evolution.

Subject headings: Galaxy: Open Clusters and Associations: Individual: Name: Hyades, Stars: Abundances

¹Data presented herein were obtained at the W. M. Keck Observatory, which is operated as a scientific partnership among the California Institute of Technology, the University of California, and the National Aeronautics and Space Administration. The Observatory was made possible by the generous financial support of the W.M. Keck Foundation.

1. Introduction

Open clusters provide an ideal opportunity to test our understanding of stellar structure and evolution. Within a given cluster, the individual stars may span a considerable range in mass and evolutionary state. Cluster stars are believed to have formed at the same time from a chemically homogeneous reservoir of gas. The Hyades open cluster has been the focus of many studies due to its proximity and the importance of the Hyades extends beyond stellar structure and evolution. The seminal papers by Perryman et al. (1998) and de Bruijne et al. (2001) address key issues including membership, distance, and age as well as outlining the prominent role played by the Hyades over the past century.

While it had been assumed that all stars within a cluster have the same composition, Conti et al. (1965) were the first to show that cluster stars are chemically homogeneous (with Li (Boesgaard & Tripicco 1986) and Be (Boesgaard & King 2002) being notable exceptions) through an analysis of 10 Hyades dwarfs. As a result of the first dredge up, cluster subgiants and giants will have different compositions than unevolved stars. Varenne & Monier (1999) review the subsequent abundance determinations for Hyades stars. Recently, Paulson et al. (2003) have confirmed the uniformity of the iron abundance through an analysis of 55 Hyades dwarfs with spectral types ranging from F to K. Paulson et al. have also shown that within the measurement uncertainties, the abundance ratios of Na, Mg, Si, Ca, Ti, and Zn with respect to Fe are constant (at the $1\sigma = 0.04$ dex level) and in their solar proportions.

In this paper, we utilize the chemical homogeneity of Hyades stars to study 2 related issues. The primary question we seek to answer is whether or not Hyades stars have uniform Mg isotopic ratios? In Yong et al. (2003b), we measured the Mg isotope ratios in cool field dwarfs to study Galactic chemical evolution. There was a scatter in the isotope ratios at a fixed $[\text{Fe}/\text{H}]$ and a hint of an increasing ratio with decreasing T_{eff} . It was also curious that the 2 stars with remarkably high ratios of $^{25,26}\text{Mg}/^{24}\text{Mg}$ had particularly strong MgH lines. Our assumption is that the true Mg isotope ratios are uniform in Hyades dwarfs. An observational contradiction of this assumption is here taken as a failure of the analytical technique. The second concern to be addressed is how appropriate are the model atmospheres and the assumptions underpinning the analysis when studying cool stars? The analysis of a chemically homogeneous sample of stars spanning a broad range in effective temperature (T_{eff}) is a powerful test of a model atmosphere grid and the analysis techniques. Departures from local thermodynamic equilibrium (LTE) may manifest as T_{eff} -dependent abundance anomalies. In particular, we note that Feltzing & Gustafsson (1998), Schuler et al. (2003) and Allende Prieto et. al (2003, private communication) have studied cool stars and found an overionization of Fe with respect to the LTE predictions. The degree of overionization increases with decreasing T_{eff} . All these studies rely upon classical one-dimensional LTE model

atmospheres. Recent advances in model atmospheres include non-local thermodynamic equilibrium (Non-LTE) models (e.g. Hauschildt et al. 1999) and LTE three-dimensional time-dependent hydrodynamical models (e.g. Asplund et al. 2000). Unfortunately, construction of these new models requires large amounts of computing time and, therefore, such models only cover a small range of stellar parameters.

Abundance analyses of cool stars are rare, and no previous study of the Hyades has investigated stars cooler than $T_{\text{eff}} \simeq 4800\text{K}$. Hyades stars are perfect targets for investigating any dependence of the Mg isotope ratios upon T_{eff} as well as identifying whether the problem of overionization of Fe exists in cool Hyades dwarfs when using classical model atmospheres. Here we measure the Mg isotope ratios in 32 Hyades dwarfs with $4000\text{K} \leq T_{\text{eff}} \leq 5000\text{K}$. (For stars warmer than 5000K, the MgH lines – from which the Mg isotope ratios are measured – are too weak.) We also determine stellar parameters and iron abundances for 56 Hyades dwarfs with $4000\text{K} \leq T_{\text{eff}} \leq 6200\text{K}$. This is the first study of the Mg isotope ratios in an open cluster and incorporates the coolest Hyades stars to which detailed spectroscopic abundance analyses have been applied.

2. Observations and data reduction

The stars in this paper are a subset of those being analyzed as part of a planet search program. For the complete description of observations and candidate selection, see Cochran et al. (2002). The observations were made using HIRES (Vogt et al. 1994) on the Keck I telescope between 1996 and 2002 with a resolving power of $R \equiv \lambda/\Delta\lambda = 60,000$. The wavelength range (3800 to 6200Å) was selected to include I₂ absorption lines and to monitor stellar chromospheric activity in Ca II H and K lines as required by the radial velocity program. The spectra used in this study are the “template” spectra which were taken without the I₂ cell in the stellar beam and therefore are free of I₂ absorption lines. The signal-to-noise ratio (S/N) ranged from 80 to 200 per pixel at 5140Å. The MgH lines from which the Mg isotope ratios will be derived are located at 5140Å. One dimensional wavelength calibrated normalized spectra were extracted in the standard way using the IRAF² package of programs.

²IRAF is distributed by the National Optical Astronomy Observatories, which are operated by the Association of Universities for Research in Astronomy, Inc., under cooperative agreement with the National Science Foundation.

3. Stellar parameters and the iron abundance

T_{eff} were determined using the Alonso et al. (1996) $T_{\text{eff}}:[\text{Fe}/\text{H}]:\text{color}$ relations based on the infrared flux method. We used the Strömrgren $b - y$ index and the $B - V$ index where Alonso et al. state that the standard deviation from the fits are 110K and 130K respectively. We have $B - V$ (Allende Prieto & Lambert 1999) for all stars and $b - y$ (Hauck & Mermilliod 1998) for 32 of the 56 stars. We applied the Alonso et al. $T_{\text{eff}}:[\text{Fe}/\text{H}]:\text{color}$ relations to determine T_{eff} using both color indices assuming a metallicity $[\text{Fe}/\text{H}]=0.10$. If we adopt the Paulson et al. (2003) metallicity $[\text{Fe}/\text{H}]=0.13$, the values for T_{eff} would change by 5K. For the 32 stars with $B - V$ and $b - y$ photometry, we adopted the mean T_{eff} . For these 32 stars, we found that $\langle T_{\text{eff}b-y} - T_{\text{eff}B-V} \rangle = 24\text{K}$ ($\sigma = 60\text{K}$). For the remaining stars with only $B - V$ photometry, we adopted $T_{\text{eff}B-V} + 10\text{K}$.

In order to determine the surface gravity, we used the 600 Myr solar metallicity Y^2 isochrones calculated by Yi et al. (2001). (Perryman et al. (1998) have shown that the Hyades have an age 625 ± 50 Myr.) We fitted a spline function through the $\log g$ and T_{eff} values given in the isochrone and assumed the gravity corresponding to the adopted T_{eff} . If we use the 800 Myr solar metallicity isochrones, the gravities would only change by 0.01 dex.

Equivalent widths (EWs) were measured for a selection of 20 Fe I and 9 Fe II lines using IRAF where in general Gaussian profiles were fit to the observed profile. These lines were identical to those used by Paulson et al. (2003) and are presented in Table 1. The gf values were taken from Kurucz & Bell (1995), Lambert et al. (1996), Schnabel et al. (2003), and from a compilation by R.E. Luck (1993, private communication). The solar Fe abundance was derived from a solar spectrum (of Ceres) taken through HIRES. Due to instrumental effects, there was a difference of 0.10 dex between our derived $\log \epsilon(\text{Fe})_{\odot}$ and that found by Grevesse & Sauval (1999). For the Hyades stars, we used a line-by-line differential analysis to derive $[\text{Fe}/\text{H}]$. Such an analysis ensures that errors in the gf values do not greatly affect the derived abundances. The model atmospheres were taken from the Kurucz (1993) LTE stellar atmosphere grid. We interpolated within the grid when necessary to produce a model with the required T_{eff} , $\log g$, and $[\text{Fe}/\text{H}]$. The model was used in the LTE stellar line analysis program MOOG (Snedden 1973). The microturbulence (ξ_t) was determined in the usual way by insisting that the Fe abundance from Fe I lines be independent of their equivalent width (W_{λ}). See Figure 1 for an example of how the abundance versus W_{λ} plot is used to set ξ_t . While this method worked for the warmer stars, we encountered problems with stars cooler than about 4900K where no value of ξ_t would produce a zero trend in the abundance versus W_{λ} plot. Feltzing & Gustafsson (1998) report a similar problem where “for the K dwarf stars none of the described methods seemed to yield definite values for the microturbulence parameter”. For these stars, we adopted a microturbulence of 0.3 km s^{-1} , a value which

reduced (but did not eliminate) the trend in the abundance versus W_λ plot. Later in the paper we show that our results are not significantly affected by our choice of microturbulence. The stellar parameters are given in Table 2.

An alternative method for deriving T_{eff} is by forcing the abundances of individual Fe I lines to be independent of lower excitation potential. See Figure 1 for an example of how T_{eff} can be determined by requiring excitation equilibrium. While we only have 5 Fe I lines with lower excitation potentials less than 3eV, the adopted T_{eff} generally result in Fe abundances independent of lower excitation potential. Many of the stars in this study are included in de Bruijne et al. (2001) and Paulson et al. (2003) and in Figure 2 and Table 3, we compare the values for T_{eff} . On average, we find that our T_{eff} are 150K cooler than the Paulson et al. (2003) values and 140K cooler than the de Bruijne et al. (2001) values. These differences are comparable to the uncertainties arising from the application of the Alonso et al. (1996) $T_{\text{eff}}:[\text{Fe}/\text{H}]:\text{color}$ relations. We note that Paulson et al. determine T_{eff} from excitation equilibrium whereas de Bruijne et al. derive T_{eff} (for stars cooler than 7250K) from the Lejeune et al. (1998) calibrations for $T_{\text{eff}}:B - V:\log g$. If reddening significantly affected the color indices, this could explain why our T_{eff} are cooler than the Paulson et al. values, but not the de Bruijne et al. values. However, Hyades stars are not significantly reddened with $E(B - V) = 0.003 \pm 0.002$ mag (Taylor 1980).

Surface gravities can be set by requiring the Fe abundance derived from Fe I lines match the Fe abundance derived from Fe II lines, i.e., ionization equilibrium. Paulson et al. set their gravities by requiring ionization equilibrium while de Bruijne et al. use the Lejeune et al. (1998) calibrations for $T_{\text{eff}}:B - V:\log g$. In Figure 3 and Table 3, we compare the values for surface gravity. The agreement is good between the various studies where the maximum difference between this study and Paulson et al. is 0.16 dex while the maximum difference between this study and de Bruijne et al. is 0.10 dex.

A striking result of our analysis is that the Fe abundance from Fe II lines exceeds that from the Fe I lines. The excess (Figure 4) is approximately constant for $T_{\text{eff}} > 5000$ K at 0.2 dex, but increases steeply with decreasing T_{eff} reaching the remarkable value of about 1 dex at 4000 K. Edvardsson et al. (1993) and Reddy et al. (2003) studied F and G dwarfs ($5500\text{K} \leq T_{\text{eff}} \leq 6500\text{K}$) and found good, but not perfect, agreement between the abundances from neutral and ionized iron. The abundance from the Fe I lines is constant for stars hotter than about 4300 K but increases by about 0.2 dex for stars of 4000 K. Ionization equilibrium is not satisfied by our analysis. This result was anticipated by several earlier analyses but no previous analysis has examined stars as cool as 4000K.

Paulson et al. (2003) considered only stars hotter than 4700K. In this range, imposition of LTE ionization equilibrium by their spectroscopic method of determining T_{eff} and $\log g$

does not yield a result for the Fe abundance significantly different from ours. Our mean abundance for stars hotter than 4700K is $[\text{Fe}/\text{H}] = 0.16 \pm 0.02$ ($\sigma = 0.1$) where all lines were given equal weight. In Table 4, we present the abundance dependences upon the model parameters. (Note that our choice of microturbulence and the adopted surface gravity do not significantly affect the results.) Our abundance difference from neutral and ionized lines for these warm stars vanishes with a temperature correction of around 150K or a change of $\log g$ by 0.5 dex. The T_{eff} adjustment is not implausible, but the gravity reduction of 0.5 dex may be rejected as inconsistent with the gravity predicted by the evolutionary tracks. Application of the temperature correction raises the mean Fe abundance by about 0.1 dex.

Schuler et al. (2003) studied dwarfs in the open cluster M 34 using high-resolution spectra and Kurucz models with T_{eff} set by excitation equilibrium of Fe I lines and surface gravities estimated from an empirical relation. Their stars covered the temperature range from 4700 to 6200K. At 6200K, the Fe abundance from the neutral lines is about 0.15 dex higher than that from the ionized lines, but at 4700K the ionized lines give the higher abundance by about 0.6 dex. These results are in reasonable agreement with those in Figure 4.

Feltzing & Gustafsson (1998) found overionization ($[\text{Fe}/\text{H}]_{\text{II}} - [\text{Fe}/\text{H}]_{\text{I}} \simeq 0.3 - 0.4$) for five K dwarfs in the range $4510\text{K} \leq T_{\text{eff}} \leq 4833\text{K}$ with no obvious trend with T_{eff} . They considered the possibility that the T_{eff} scale may be in error and concluded that departures from LTE are a likely cause of the discrepancy. Thorén & Feltzing (2000) reanalyzed the five problematic K dwarfs. Use of a T_{eff} scale based on excitation equilibrium rather than photometric temperatures changed the T_{eff} of 1 star by +200K. By fitting the wings of strong lines, surface gravities were changed in the remaining stars by 0.3 to 0.5 dex. Synthetic spectra allowed for revision of the continuum and a different linelist was employed. Modification of their analysis techniques showed that the overionization of Fe was small, $[\text{Fe}/\text{H}]_{\text{II}} - [\text{Fe}/\text{H}]_{\text{I}} \simeq 0.1$.

Figure 4 is evidence that the standard combination of a classical atmosphere and LTE physics of line formation fails to reproduce the collection of neutral and ionized iron lines in the spectra of cool dwarfs with the failure increasing with decreasing temperature.³ We used the van der Waals line damping parameter (Unsöld approximation multiplied by a factor recommended by the Blackwell group). We tested other damping parameters and none resulted in a closer agreement between the abundances from neutral and ionized iron.

³The failure cannot be eliminated by alternative sources of classical atmospheres. Use of NEXGEN (Hauschildt et al. 1999) models which include improved molecular opacities does not materially change the results in Figure 4.

A suspicion aired in previous papers is that Non-LTE effects on the ionization equilibrium between neutral Fe atoms and the singly-charged ions are responsible for discrepant abundances from Fe I and Fe II lines: iron atoms are over-ionized (relative to LTE) by the ultraviolet radiation field. Published calculations of Non-LTE effects on iron atoms and ions (e.g., Thévenin & Idiart 1999; Gehren et al. 2001; Shchukina & Trujillo Bueno 2001) for stars of approximately solar metallicity and of solar or warmer temperatures indicate the effects are small. Overionization at these temperatures, were it a large effect, would be seen most obviously as an underabundance in LTE analyses of the Fe I with very slight effects on the analyses of the Fe II; iron is predominantly singly-ionized in F and G atmospheres. These calculations use classical (LTE) atmospheres and, hence, are an incomplete characterization of the Non-LTE effects. In the atmospheres of the coolest stars of our study, neutral atoms greatly outnumber the ions and, hence, overionization can greatly increase the number of ions without significantly decreasing the number of neutral atoms. Overionization is likely driven by the flux of ultraviolet photons penetrating the line-forming regions. With or even without a chromosphere, the mean intensity of this flux (J_ν) seems certain to exceed the flux assumed in LTE (i.e., B_ν , the local Planck function). The Hyades dwarfs are chromospherically active (e.g., Wilson 1963; Duncan et al. 1984; Reid et al. 1995) and, therefore, likely to provide for greater Non-LTE effects than in comparable but older stars. Quantitative evaluation of the Non-LTE effects on iron and other elements are awaited with interest.

A possible contributor to the apparent disequilibrium of iron ionization in the coolest dwarfs is that classical model atmospheres are an inadequate representation of the real atmospheres of these dwarfs. Stellar granulation is not recognized by the classical assumptions. Spots may be prevalent on these young stars. Heating processes supporting the temperature rise of the chromosphere may affect the photospheric structure. Non-LTE effects may influence the photospheric structure.

4. Magnesium isotopic ratios

Our primary goal is to determine the Mg isotopic ratios in the Hyades dwarfs from the warmest stars in which MgH lines are of adequate strength ($T_{\text{eff}} \simeq 5000\text{K}$) to the coolest in our sample ($T_{\text{eff}} \simeq 4000\text{K}$). The working assumption is that the stars are chemically homogeneous, certainly with respect to the Mg isotopes. Initially, the principal motivation was an earlier suspicion that measured isotopic ratios from spectra of dwarfs were dependent on a star's T_{eff} (Yong et al. 2003b). With the discovery of severe ionization disequilibrium in the coolest Hyades dwarfs, the motivation for pursuing the Mg isotopic ratios was greatly strengthened.

The isotopic ratios are obtained from MgH lines near 5140\AA . Figure 5 shows a repre-

sentative spectrum of a star with strong MgH lines. At a given T_{eff} , stars have identical spectra, as illustrated in Figure 6 where we overplot the spectra of two stars with almost identical parameters. There are no discernable differences in the profiles of the MgH features suggesting that the isotopic ratios may indeed be very similar.

While many MgH lines are present in the spectra of cool stars, few are suitable for isotopic analysis (Tomkin & Lambert 1980). To measure the Mg isotope ratios, we rely upon three MgH features recommended by McWilliam & Lambert (1988) and used by Gay & Lambert (2000) and Yong et al. (2003a,b). The three lines are at 5134.6Å, 5138.7Å, and 5140.2Å and we refer to them as Region 1, 2, and 3. These lines are described in detail by McWilliam & Lambert (1988). The macroturbulence was determined by fitting the profile of an unblended line, Ti I at 5145.5Å. For all stars, this Ti I line was slightly stronger than the recommended MgH lines. The macroturbulence was assumed to have a Gaussian form representing the approximately equal contributions from atmospheric turbulence, stellar rotation, and instrumental profile. The linelist was identical to the one used by Gay & Lambert (2000) and includes contributions from C, Mg, Sc, Ti, Cr, Fe, Co, Ni, and Y. The wavelengths of all isotopic components were taken from McWilliam & Lambert (1988) and were based on direct measurements of an MgH spectrum obtained using a Fourier transform spectrometer by Bernath et al. (1985).

The abundances of ^{25}Mg and ^{26}Mg were adjusted until the profiles of the 3 recommended features were best fit. Following the work by Nissen et al. (1999, 2000) on Li isotope ratios and Yong et al. (2003a) on Mg isotope ratios, we used a χ^2 analysis to determine the best fit to the data. The advantages to this method are that it is unbiased and errors in the fits can be quantified. The free parameters were (1) $^{25}\text{Mg}/^{24}\text{Mg}$, (2) $^{26}\text{Mg}/^{24}\text{Mg}$, and (3) $\log\epsilon(\text{Mg})$ and we treated each of the three recommended features independently. We took the terrestrial ratio, $^{24}\text{Mg}:^{25}\text{Mg}:^{26}\text{Mg} = 78.99:10.00:11.01$ (de Bièvre & Barnes 1985) as our initial guess and we refer to these ratios as the solar ratios. We explored a large range of parameter space around our initial guess and calculated $\chi^2 = \Sigma(O_i - S_i)^2/\sigma^2$ where O_i is the observed spectrum point, S_i is the synthesis, and $\sigma = (S/N)^{-1}$. The optimum values for $^{25}\text{Mg}/^{24}\text{Mg}$, $^{26}\text{Mg}/^{24}\text{Mg}$, and $\log\epsilon(\text{Mg})$ were determined by locating the minima in χ^2 . We tested over 500 different synthetic spectra per region and the minimum $\chi_{red}^2 = \chi^2/\nu$, where ν is the number of degrees of freedom in the fit, was sufficiently close to 1. Examples of spectrum syntheses are shown in Figures 7 and 8 and the optimal isotope ratios are given in Table 2. Note that the red asymmetry on the MgH lines is due to the presence of ^{25}MgH and ^{26}MgH . The synthesis computed assuming only ^{24}MgH provides a poor fit to the spectrum.

Following Bevington & Robinson (1992), we plotted $\Delta\chi^2 = \chi^2 - \chi_{min}^2$ against the ratios $^{25}\text{Mg}/^{24}\text{Mg}$ and $^{26}\text{Mg}/^{24}\text{Mg}$ (see Figure 9). We took $\Delta\chi^2 = 1$ to be the 1σ confidence

limit for determining $^{25}\text{Mg}/^{24}\text{Mg}$ or $^{26}\text{Mg}/^{24}\text{Mg}$. For each region of each star, we paired an uncertainty to the optimized value for $^{25}\text{Mg}/^{24}\text{Mg}$ or $^{26}\text{Mg}/^{24}\text{Mg}$ and a weighted mean was calculated giving a single value of $^{24}\text{Mg}:^{25}\text{Mg}:^{26}\text{Mg}$ for each star (see Table 2). As stated in previous studies of the Mg isotope ratios, we find that the ratio $^{25}\text{Mg}/^{24}\text{Mg}$ is less certain than $^{26}\text{Mg}/^{24}\text{Mg}$ since ^{26}MgH is less blended with the strong ^{24}MgH line. We also find that isotope ratios from Regions 2 and 3 are less accurate than from Region 1, as noted by Yong et al. (2003a). As previously shown by McWilliam & Lambert (1988) and Yong et al. (2003a), Region 1 tends to give higher ratios than Regions 2 and 3. In calculating the mean isotope ratio for a given star, we also determine formal statistical errors ($\Delta\chi^2 = 1$). However, these errors are very small, and neglect systematic errors from continuum fitting, microturbulence, macroturbulence, identified and unidentified blends. Examination of Figures 7 and 8 show that it is difficult to discern by eye differences in the syntheses at or below the level $b \pm 3$ or $c \pm 3$ when expressing the ratio as $^{24}\text{Mg}:^{25}\text{Mg}:^{26}\text{Mg}=(100-b-c):b:c$. The derived isotope ratios are insensitive to the adopted stellar parameters (see Yong et al. 2003b for a discussion of uncertainties). For HIP 18946 we adopted a microturbulence of 0.8 km s^{-1} (originally 0.3 km s^{-1}) and measured the ratio 75:12:13 (originally 76:12:12). Even for the coolest star HIP 19082 for which the microturbulence would have the greatest effect, the ratio was 78:11:11 (originally 80:10:10) when the microturbulence was changed to 0.8 km s^{-1} (from 0.3 km s^{-1}).

In Figure 10, we plot the Mg isotope ratios $^{25}\text{Mg}/^{24}\text{Mg}$, $^{26}\text{Mg}/^{24}\text{Mg}$, and $^{26}\text{Mg}/^{25}\text{Mg}$ versus T_{eff} . None of the isotope ratios show a significant trend with T_{eff} . The mean ratio for the Hyades is $^{24}\text{Mg}:^{25}\text{Mg}:^{26}\text{Mg} = 78.6:10.1:11.3$, almost identical to the solar ratio 78.99:10.00:11.01 (de Bièvre & Barnes 1985). This demonstration that the Hyades and solar system isotopic ratios are in good agreement is not a surprise given the small difference in composition between the Hyades and Sun. In usual parlance $[\text{Fe}/\text{H}]$ is small (see above) and $[\text{X}/\text{Fe}]$ is zero to within small measurement errors for all elements (except Li and Be) examined. What may be a surprise given the results in Figure 4 is that the Hyades Mg isotope ratios are quite independent of T_{eff} . This result will serve to test explanations of Figure 4.

Classical atmospheres assume homogenous layers. Should the real atmosphere consist of hot and cool columns, MgH lines will be strong in the cool columns and weak in the hot columns. The continuum from hot columns will weaken the MgH lines from the cool columns. The analysis of the combined spectrum using a classical atmosphere will lead to an underestimate of the saturation and an overestimate of the ratios $^{25}\text{Mg}/^{24}\text{Mg}$ and $^{26}\text{Mg}/^{24}\text{Mg}$. Lambert et al. (1971) showed that this effect was responsible for producing artificially high Mg isotope ratios reported from sunspot spectra. Thus, it would be useful to measure the Mg isotope ratios using a three-dimensional hydrodynamic model atmosphere. The youth of the Hyades may give rise to a significant fraction of starspot coverage.

Normally we avoid using the MgH features to determine the Mg abundance. Slight variations in the adopted temperature can result in large changes in the derived Mg abundance. Uncertainties in the absolute gf -values of the MgH lines and the molecule’s dissociation energy will also introduce a systematic offset in the derived abundances. We plot the Mg abundances versus T_{eff} in Figure 11 and find that the abundance decreases with decreasing T_{eff} . If we plot $[\text{Mg}/\text{Fe I}]$ (where Fe I is the iron abundance from neutral species) the trend of Mg with T_{eff} would be even more pronounced. For HIP 19098 ($T_{\text{eff}}=4978\text{K}$) and HIP 18946 ($T_{\text{eff}}=4485\text{K}$), we increased the adopted T_{eff} by 150K and found that the Mg abundance increased by about 0.3 dex. Therefore, in the warmer stars, the 150K adjustment brings the Mg abundance from MgH lines into agreement with the Paulson et al. values as well as reproducing ionization equilibrium. However, in our cooler stars, the 150K adjustment does not result in agreement with the Paulson et al. Mg abundances, the trend of $[\text{Mg}/\text{H}]$ with T_{eff} does not disappear, and iron ionization equilibrium is not satisfied. (The Paulson et al. Mg abundances are derived from atomic Mg lines.) The anticorrelation seen in Figures 4 and 11 suggests that the mechanisms responsible for the apparent overionization of Fe also affect the Mg abundances in the coolest stars.

5. Concluding remarks

We measured the Mg isotope ratios in 32 dwarfs with $4000\text{K} \leq T_{\text{eff}} \leq 5000\text{K}$. Our goal was to investigate whether our analysis was susceptible to problems in the model atmospheres or analysis. In Yong et al. (2003b) the two stars with high ratios of $^{25}\text{Mg}/^{24}\text{Mg}$ were rather cool and there was a hint that the Mg isotope ratios showed a trend with T_{eff} . (We note that these two stars were metal-poor relative to the Hyades.) Use of the Mg isotope ratios to investigate the chemical history of our Galaxy would be severely weakened if a temperature bias exists. It is reassuring that in the Hyades stars, we find no trend with T_{eff} . The stars in this study have MgH lines of comparable strength to the two cool stars with high isotope ratios identified by Yong et al. (2003b). The mean Mg isotope ratio for the Hyades is in excellent agreement with the solar value which is unsurprising since the Hyades have been shown to have elemental abundance ratios in accord with the solar ratios.

We also determined the stellar parameters and iron abundances for 56 Hyades dwarfs with $4000\text{K} \leq T_{\text{eff}} \leq 6200\text{K}$. For stars warmer than 4700K, we found a mean Fe abundance in good agreement with previous studies. The Fe abundance from Fe II lines was slightly higher than from Fe I lines. Modest adjustments to the stellar parameters would result in the same Fe abundance from neutral and ionized lines. Below 4700K, we found overionization of Fe where the effect increased with decreasing T_{eff} . Unrealistic changes to the adopted stellar

parameters would be required to satisfy ionization equilibrium. Similar problems have been seen by Feltzing & Gustafsson (1998), Schuler et al. (2003), and Allende Prieto et. al (2003, private communication) and all studies rely upon classical model atmospheres. None of the previous studies considered dwarfs as cool as those investigated in this study. We identify the problem of apparent overionization in cool Hyades dwarfs but offer no definitive explanation. It is likely that inadequacies in the model atmospheres and neglect of Non-LTE and/or other effects are to blame. Even though the models fail to satisfy ionization equilibrium, our Mg isotope ratios do not show any such problem. Abundance ratios determined via the analysis of identical transitions in essentially identical species are insensitive to errors in the model atmospheres or analysis.

In order to further investigate this problem of overionization of Fe, we intend to undertake a more complete abundance analysis of the Hyades focusing upon more elements (neutral and singly-charged ions where possible) as well as abundances from molecular lines. A parallel study of members of the Pleiades, other open clusters, and field stars should also be conducted. Such a study may reveal how age and metallicity influence the mechanism responsible for the overionization of Fe.

We thank Bill Cochran and Artie Hatzes for providing the data. We thank the anonymous referee for helpful comments that improved the clarity of the paper. We acknowledge support from the Robert A. Welch Foundation of Houston, Texas. This research has made use of the SIMBAD database, operated at CDS, Strasbourg, France and NASA’s Astrophysics Data System.

REFERENCES

- Allende Prieto, C. & Lambert, D. L. 1999, *A&A*, 352, 555
- Alonso, A., Arribas, S., & Martínez-Roger, C. 1996, *A&A*, 313, 873
- Asplund, M., Nordlund, Å., Trampedach, R., Allende Prieto, C., & Stein, R. F. 2000, *A&A*, 359, 729
- Bernath, P. F., Black, J. H., & Brault, J. W. 1985, *ApJ*, 298, 375
- Bevington, P. R. & Robinson, D. K. 1992, *Data reduction and error analysis for the physical sciences* (New York: McGraw-Hill, 1992, 2nd ed.)
- Boesgaard, A. M. & King, J. R. 2002, *ApJ*, 565, 587

- Boesgaard, A. M. & Tripicco, M. J. 1986, *ApJ*, 302, L49
- Cochran, W. D., Hatzes, A. P., & Paulson, D. B. 2002, *AJ*, 124, 565
- Conti, P. S., Wallerstein, G., & Wing, R. F. 1965, *ApJ*, 142, 999
- de Bièvre, P. & Barnes, I. L. 1985, *Int. J. Mass Spectrom. Ion Processes*, 65, 211
- de Bruijne, J. H. J., Hoogerwerf, R., & de Zeeuw, P. T. 2001, *A&A*, 367, 111
- Duncan, D. K., Frazer, J., Lanning, H. H., Baliunas, S. L., Noyes, R. W., & Vaughan, A. H. 1984, *PASP*, 96, 707
- Edvardsson, B., Andersen, J., Gustafsson, B., Lambert, D. L., Nissen, P. E., & Tomkin, J. 1993, *A&A*, 275, 101
- Feltzing, S. & Gustafsson, B. 1998, *A&AS*, 129, 237
- Gay, P. L. & Lambert, D. L. 2000, *ApJ*, 533, 260
- Gehren, T., Korn, A. J., & Shi, J. 2001, *A&A*, 380, 645
- Grevesse, N. & Sauval, A. J. 1999, *A&A*, 347, 348
- Hauck, B. & Mermilliod, M. 1998, *A&AS*, 129, 431
- Hauschildt, P. H., Allard, F., & Baron, E. 1999, *ApJ*, 512, 377
- Kurucz, R. 1993, *ATLAS9 Stellar Atmosphere Programs and 2 km/s grid*. Kurucz CD-ROM No. 13. Cambridge, Mass.: Smithsonian Astrophysical Observatory, 1993., 13
- Kurucz, R. & Bell, B. 1995, *Atomic Line Data (R.L. Kurucz and B. Bell)* Kurucz CD-ROM No. 23. Cambridge, Mass.: Smithsonian Astrophysical Observatory, 1995., 23
- Lambert, D. L., Heath, J. E., Lemke, M., & Drake, J. 1996, *ApJS*, 103, 183
- Lambert, D. L., Mallia, E. A., & Petford, A. D. 1971, *MNRAS*, 154, 265
- Lejeune, T., Cuisinier, F., & Buser, R. 1998, *A&AS*, 130, 65
- McWilliam, A. & Lambert, D. L. 1988, *MNRAS*, 230, 573
- Nissen, P. E., Asplund, M., Hill, V., & D’Odorico, S. 2000, *A&A*, 357, L49
- Nissen, P. E., Lambert, D. L., Primas, F., & Smith, V. V. 1999, *A&A*, 348, 211

- Paulson, D. B., Sneden, C., & Cochran, W. D. 2003, *AJ*, 125, 3185
- Perryman, M. A. C., Brown, A. G. A., Lebreton, Y., Gomez, A., Turon, C., de Strobel, G. C., Mermilliod, J. C., Robichon, N., Kovalevsky, J., & Crifo, F. 1998, *A&A*, 331, 81
- Reddy, B. E., Tomkin, J., Lambert, D. L., & Allende Prieto, C. 2003, *MNRAS*, 340, 304
- Reid, N., Hawley, S. L., & Mateo, M. 1995, *MNRAS*, 272, 828
- Schnabel, R., Schultz-Johanning, M., & Kock, M. 2003, *astro-ph/0309023*
- Schuler, S. C., King, J. R., Fischer, D. A., Soderblom, D. R., & Jones, B. F. 2003, *AJ*, 125, 2085
- Shchukina, N. & Trujillo Bueno, J. 2001, *ApJ*, 550, 970
- Sneden, C. 1973, *ApJ*, 184, 839
- Taylor, B. J. 1980, *AJ*, 85, 242
- Thévenin, F. & Idiart, T. P. 1999, *ApJ*, 521, 753
- Thorén, P. & Feltzing, S. 2000, *A&A*, 363, 692
- Tomkin, J. & Lambert, D. L. 1980, *ApJ*, 235, 925
- Varenne, O. & Monier, R. 1999, *A&A*, 351, 247
- Vogt, S. S., Allen, S. L., Bigelow, B. C., Bresee, L., Brown, B., Cantrall, T., Conrad, A., Couture, M., Delaney, C., Epps, H. W., Hilyard, D., Hilyard, D. F., Horn, E., Jern, N., Kanto, D., Keane, M. J., Kibrick, R. I., Lewis, J. W., Osborne, J., Pardeilhan, G. H., Pfister, T., Ricketts, T., Robinson, L. B., Stover, R. J., Tucker, D., Ward, J., & Wei, M. Z. 1994, in *Proc. SPIE Instrumentation in Astronomy VIII*, David L. Crawford; Eric R. Craine; Eds., Volume 2198, p. 362
- Wilson, O. C. 1963, *ApJ*, 138, 832
- Yi, S., Demarque, P., Kim, Y., Lee, Y., Ree, C. H., Lejeune, T., & Barnes, S. 2001, *ApJS*, 136, 417
- Yong, D., Grundahl, F., Lambert, D. L., Nissen, P. E., & Shetrone, M. D. 2003a, *A&A*, 402, 985
- Yong, D., Lambert, D. L., & Ivans, I. I. 2003b, *ApJ* in press (*astro-ph/0309079*)

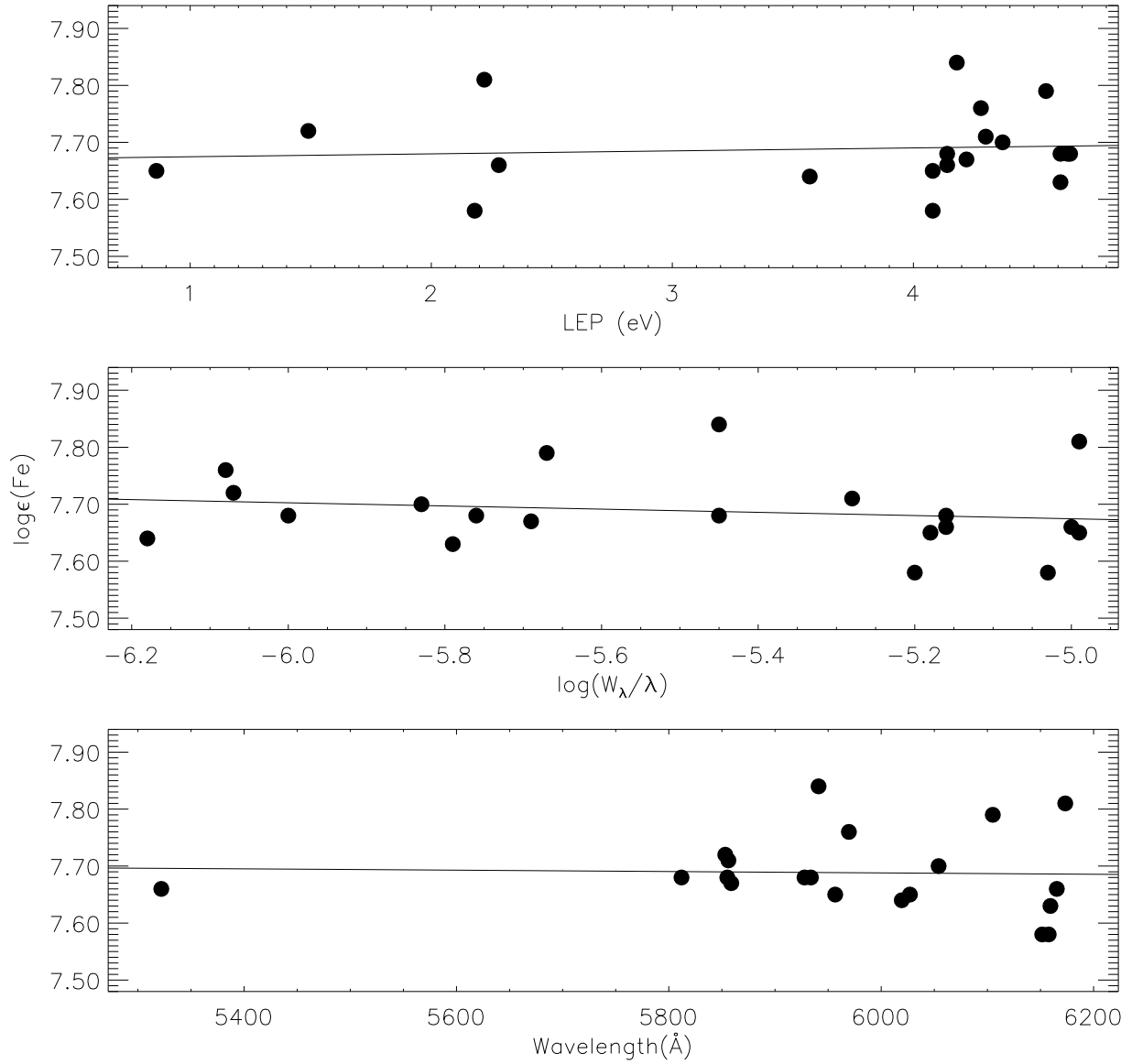


Fig. 1.— Fe abundance from individual FeI lines versus excitation potential (upper), reduced equivalent width (middle), and wavelength (lower). The lower excitation potential (LEP)-abundance relation can be used to set T_{eff} and the reduced equivalent width (W_λ/λ)-abundance relation is used to determine ξ_t . In all panels the line represents the linear least-squares fit to the data.

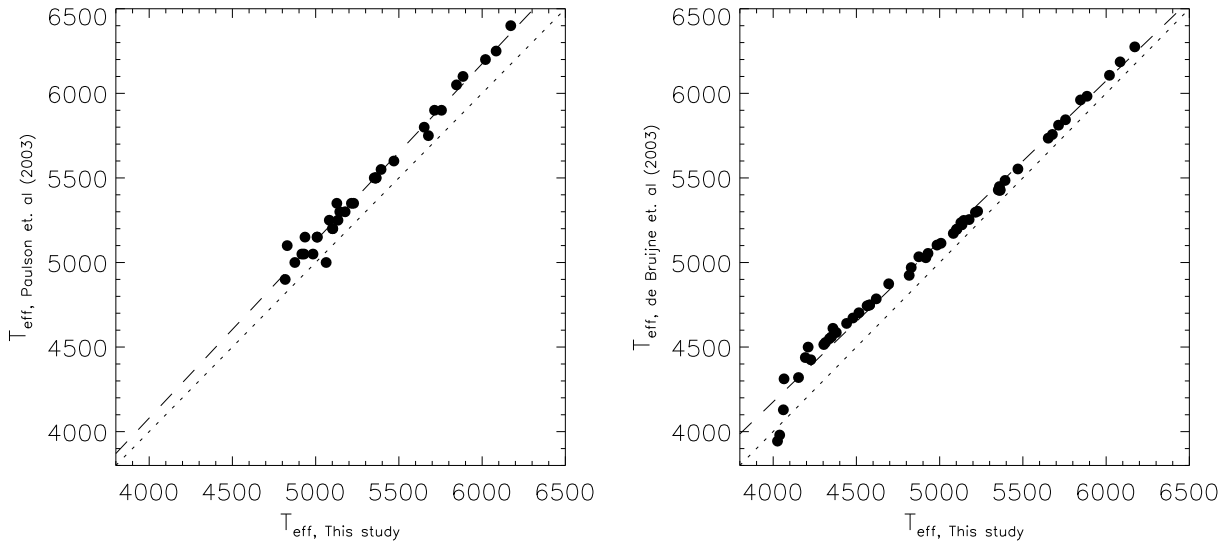


Fig. 2.— T_{eff} comparison between this study and Paulson et al. (2003) (left) and de Bruijne et al. (2001) (right). The dotted line represents the line of equality while the dashed line is the linear least-squares fit to the data.

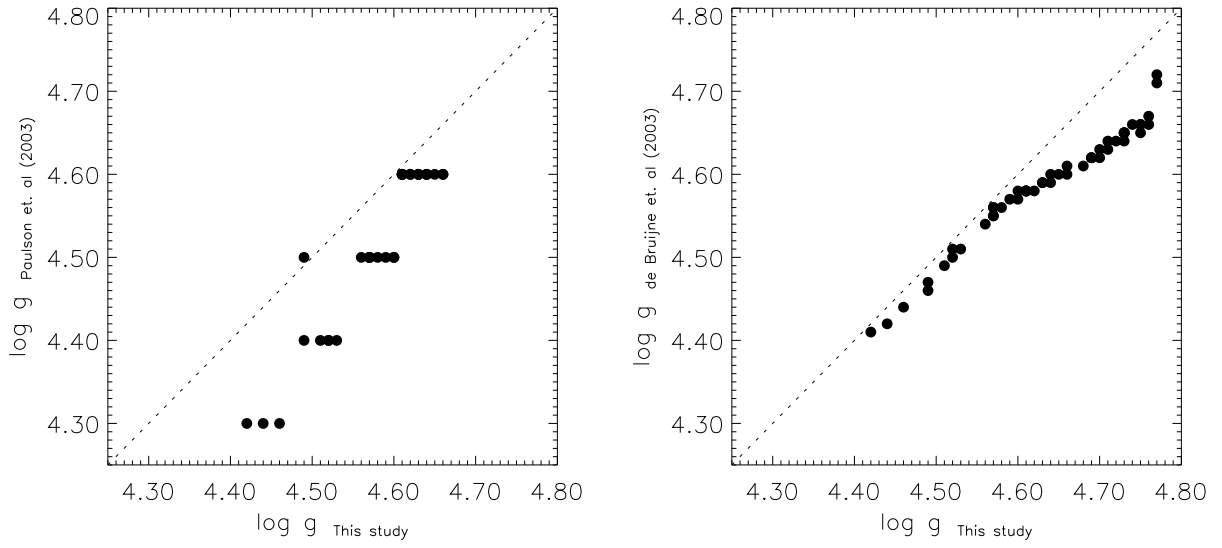


Fig. 3.— Gravity comparison between this study and Paulson et al. (2003) (left) and de Bruijne et al. (2001) (right). The dotted line represents the line of equality.

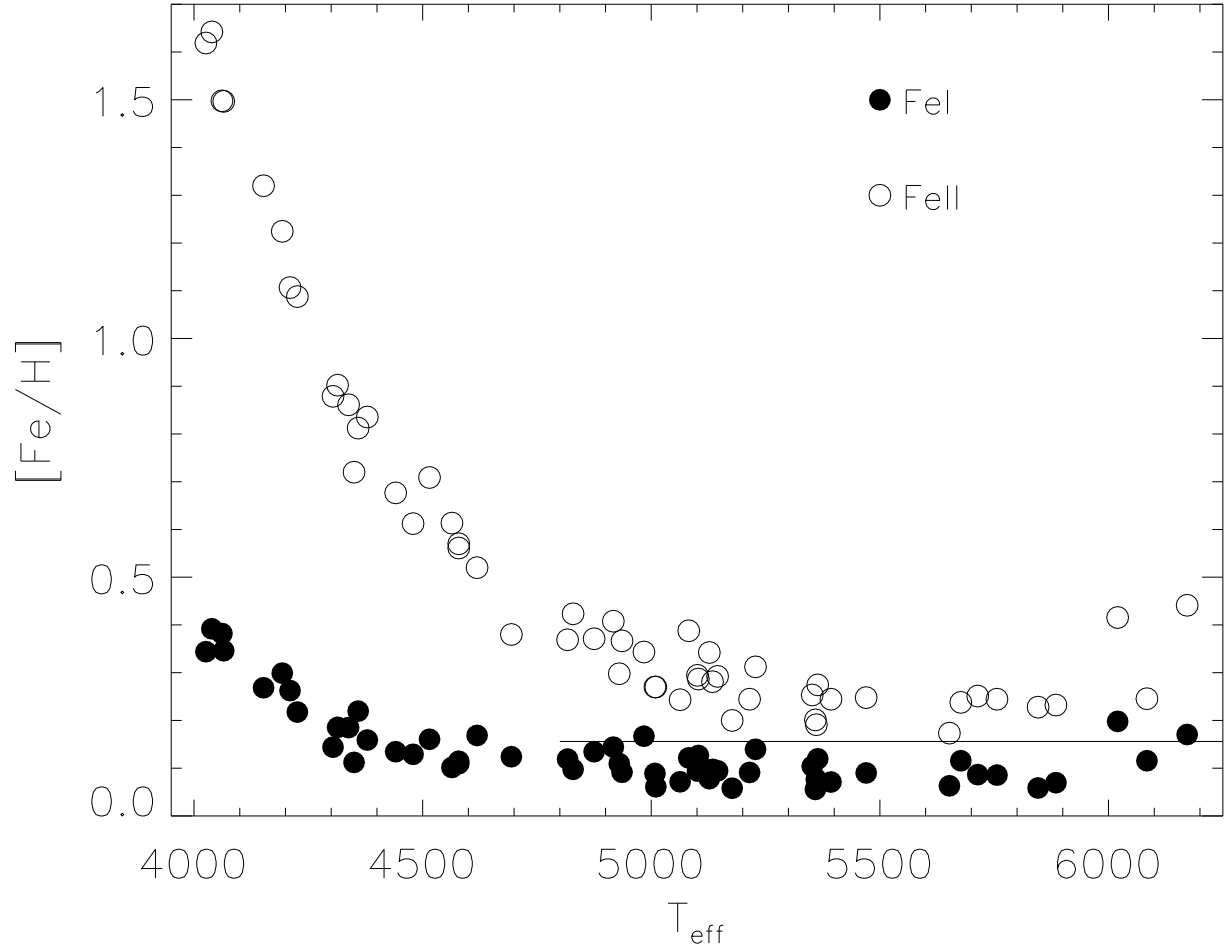


Fig. 4.— Mean Fe abundance from Fe I and Fe II lines versus T_{eff} . Above 4700K, the difference between Fe I and Fe II is constant at about 0.2 dex while below 4700K, the difference between Fe I and Fe II increases with decreasing metallicity. The solid line is the mean value of Fe based only on stars with $T_{\text{eff}} > 4700$ K.

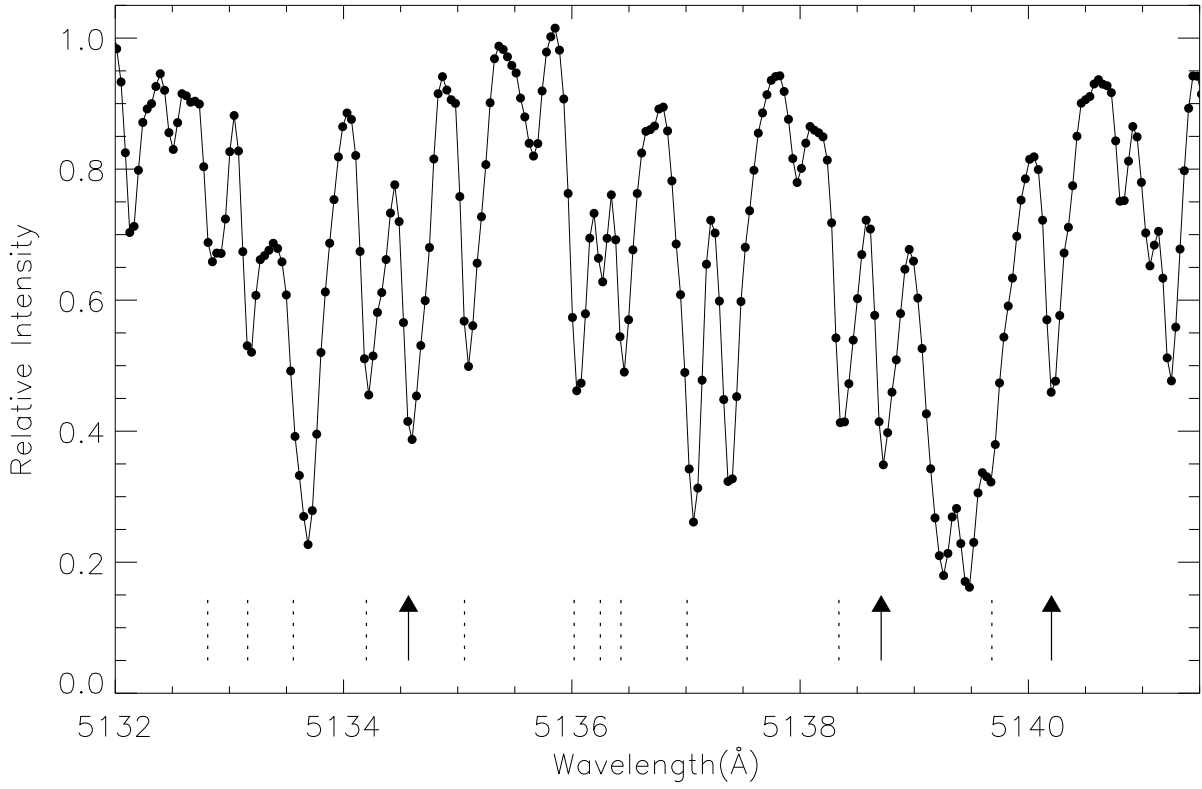


Fig. 5.— Spectrum of HIP 18322 showing the positions of various MgH lines. While most of the MgH lines are unsuitable for isotopic analysis, 3 features we use to derive the isotope ratios are marked by arrows.

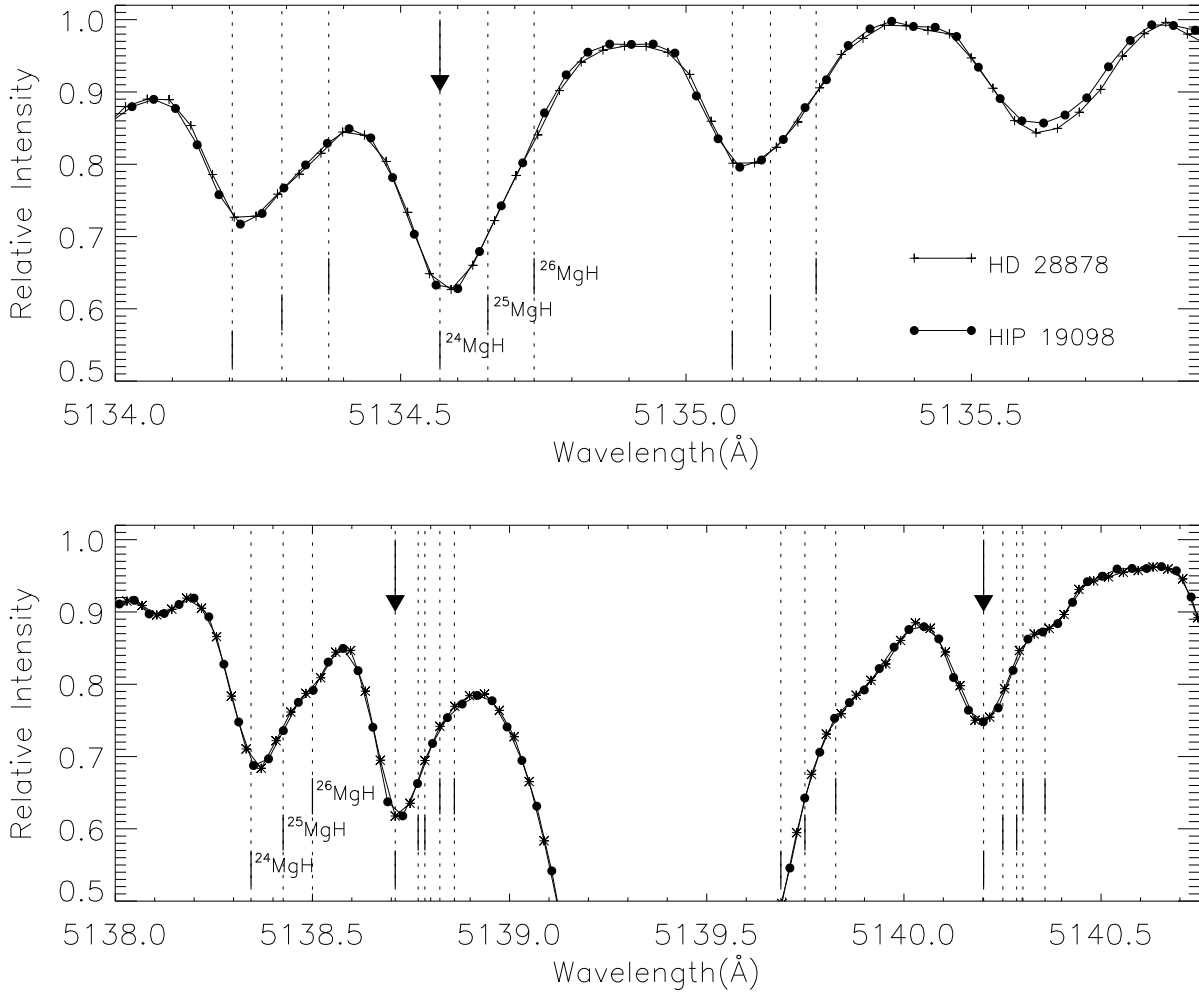


Fig. 6.— Spectra of HD 28878 and HIP 19098. The positions of the ^{24}MgH , ^{25}MgH , and ^{26}MgH lines are shown and the lines used to derive the isotope ratios are highlighted by arrows. There are no discernable differences in the profiles of the MgH lines suggesting that both stars have similar Mg isotope ratios.

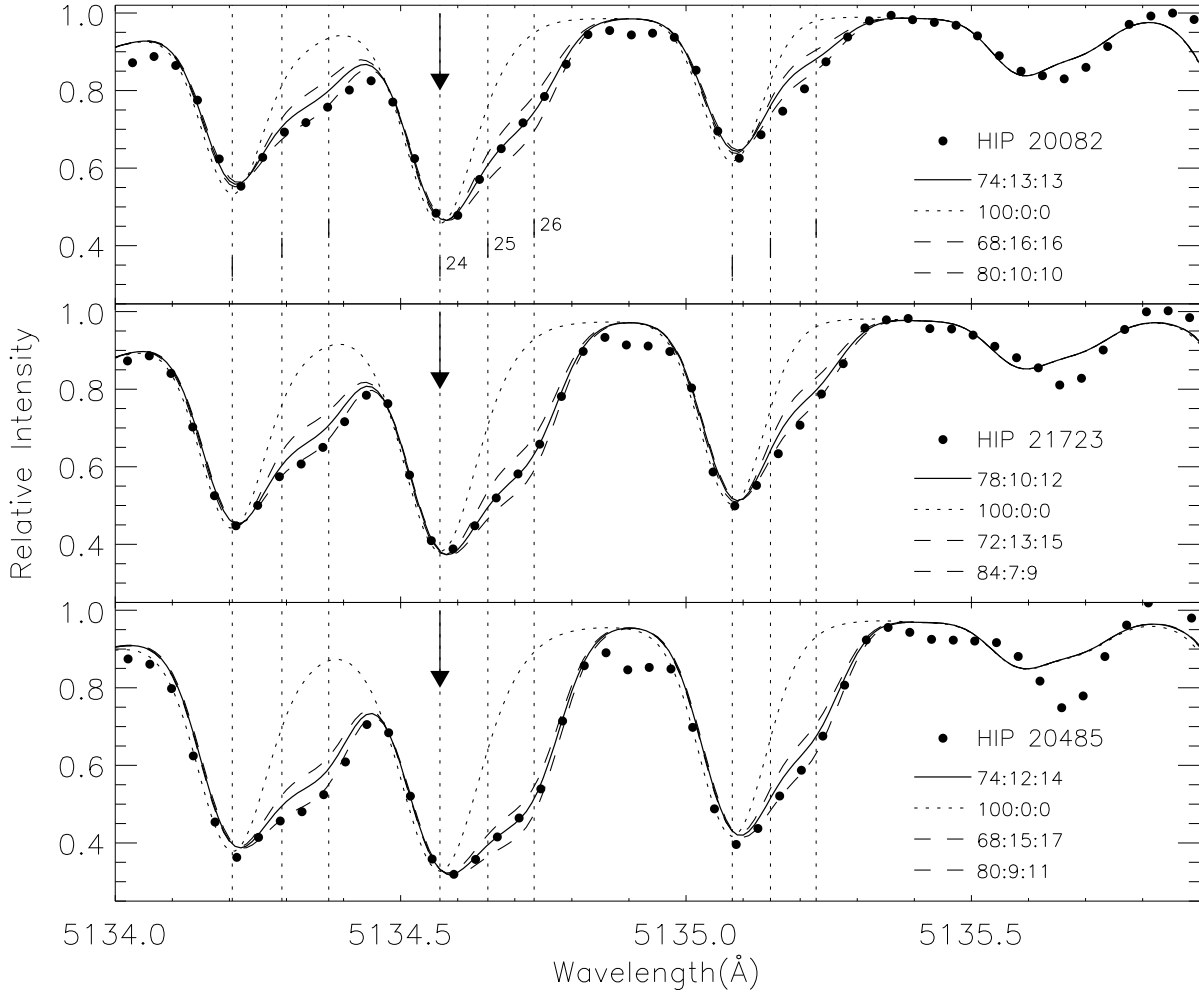


Fig. 7.— Spectra of HIP 20082, HIP 21723, and HIP 20485. The feature we are fitting is highlighted by the arrow. The positions of the ^{24}MgH , ^{25}MgH , and ^{26}MgH lines are indicated by dashed lines. The closed circles represent the observed spectra, the best fit is the solid line, and unsatisfactory ratios are also shown.

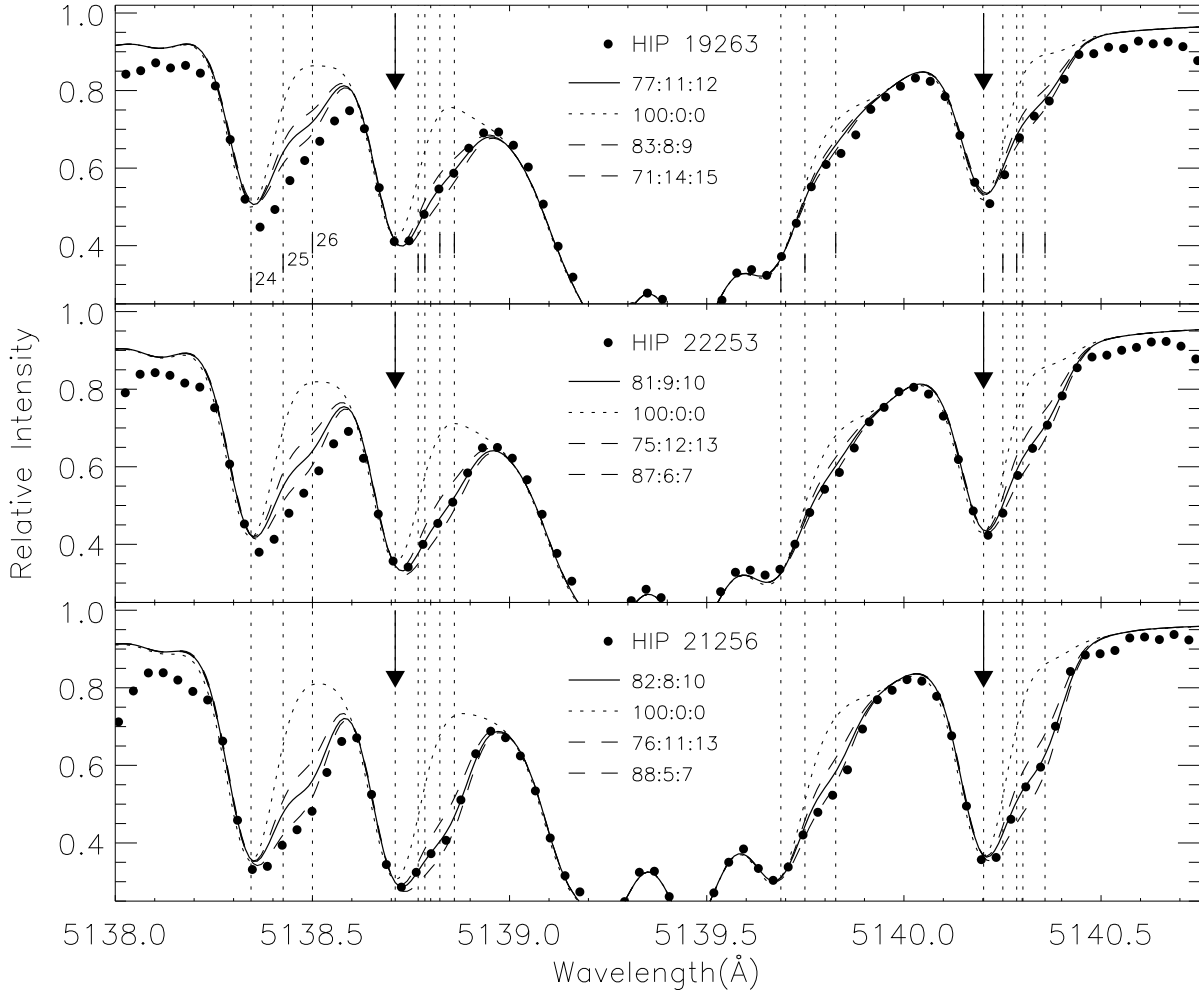


Fig. 8.— Spectra of HIP 19263, HIP 22253, and HIP 21256. The features we are fitting are highlighted by the arrows. The positions of the ^{24}MgH , ^{25}MgH , and ^{26}MgH lines are indicated by dashed lines. The closed circles represent the observed spectra, the best fit is the solid line, and unsatisfactory ratios are also shown.

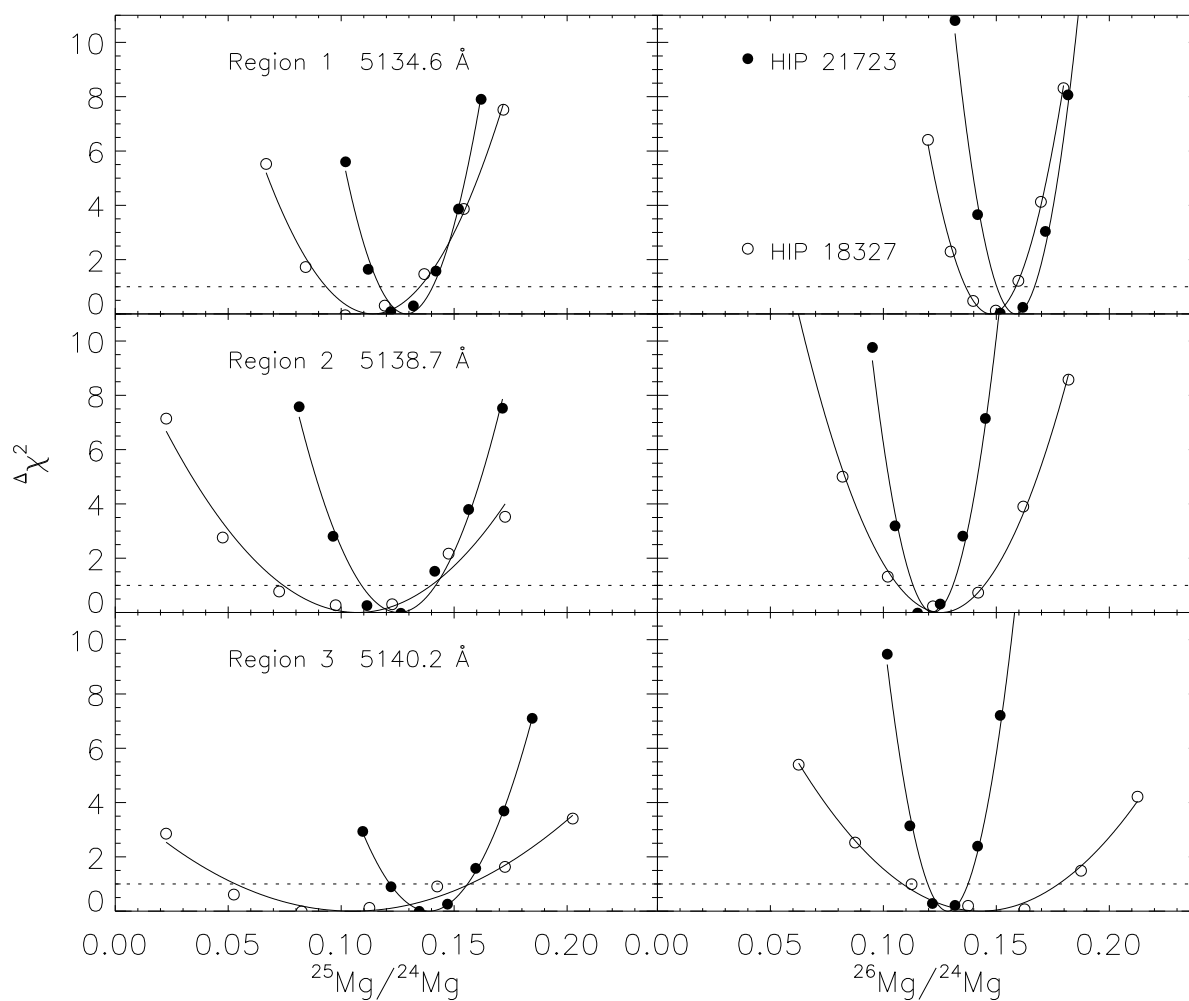


Fig. 9.— Variation in $\Delta\chi^2$ fit for HIP 21723 and HIP 18327 for $^{25}\text{Mg}/^{24}\text{Mg}$ (left panels) and $^{26}\text{Mg}/^{24}\text{Mg}$ (right panels). The upper, middle, and lower panels show the χ^2 variation for Region 1 (5134.6Å), Region 2 (5138.7Å), and Region 3 (5140.2Å). The line indicating 1σ errors ($\Delta\chi^2 = 1$) is shown.

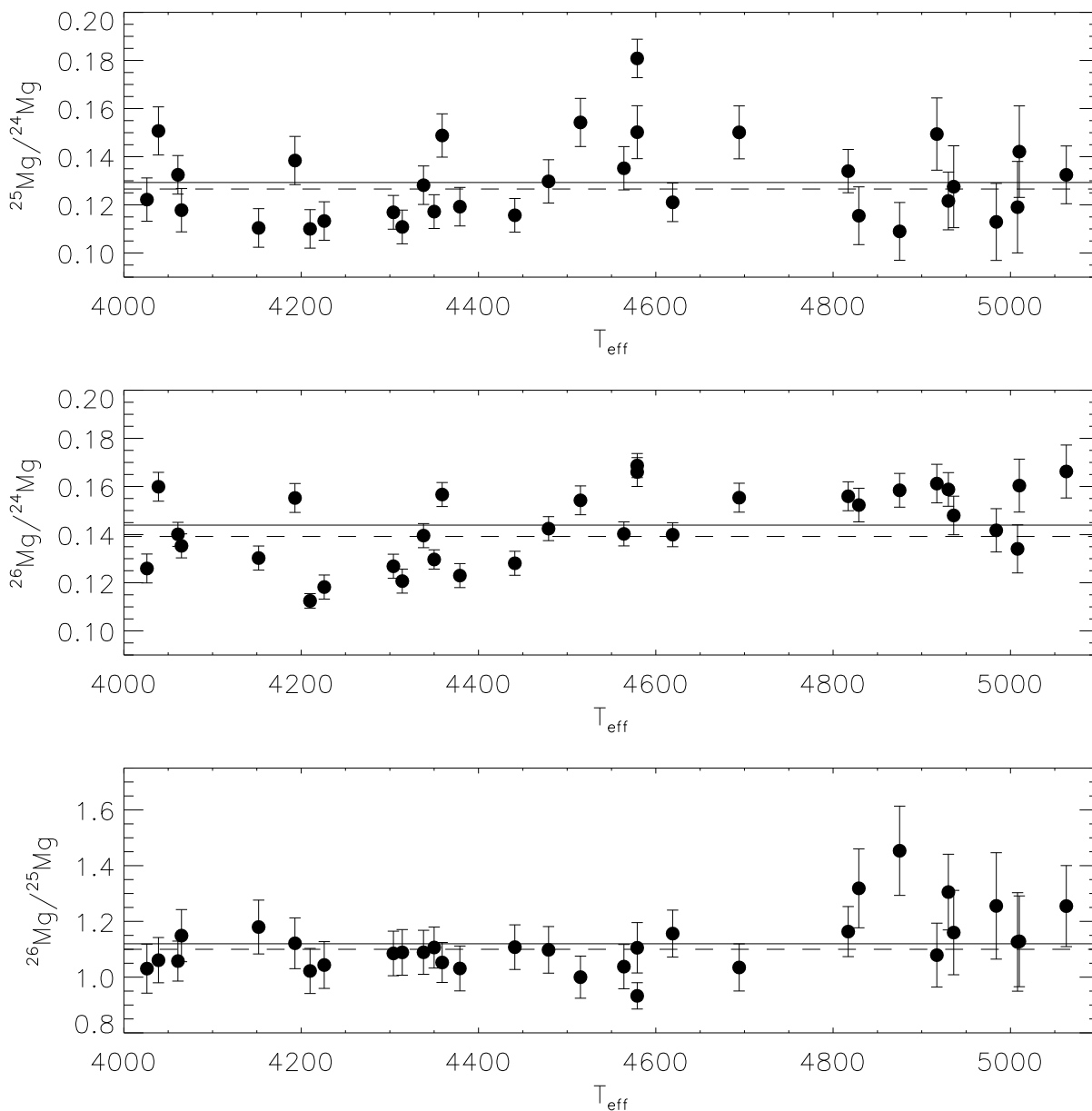


Fig. 10.— Mg isotope ratio $^{25}\text{Mg}/^{24}\text{Mg}$ (upper), $^{26}\text{Mg}/^{24}\text{Mg}$ (middle), and $^{26}\text{Mg}/^{25}\text{Mg}$ (lower) versus T_{eff} . The solid line represents the mean value and the dashed line represents the solar value. The error bars show the formal statistical errors which almost certainly underestimate the true errors (see discussion in text). There is no significant trend of any isotope ratio with T_{eff} .

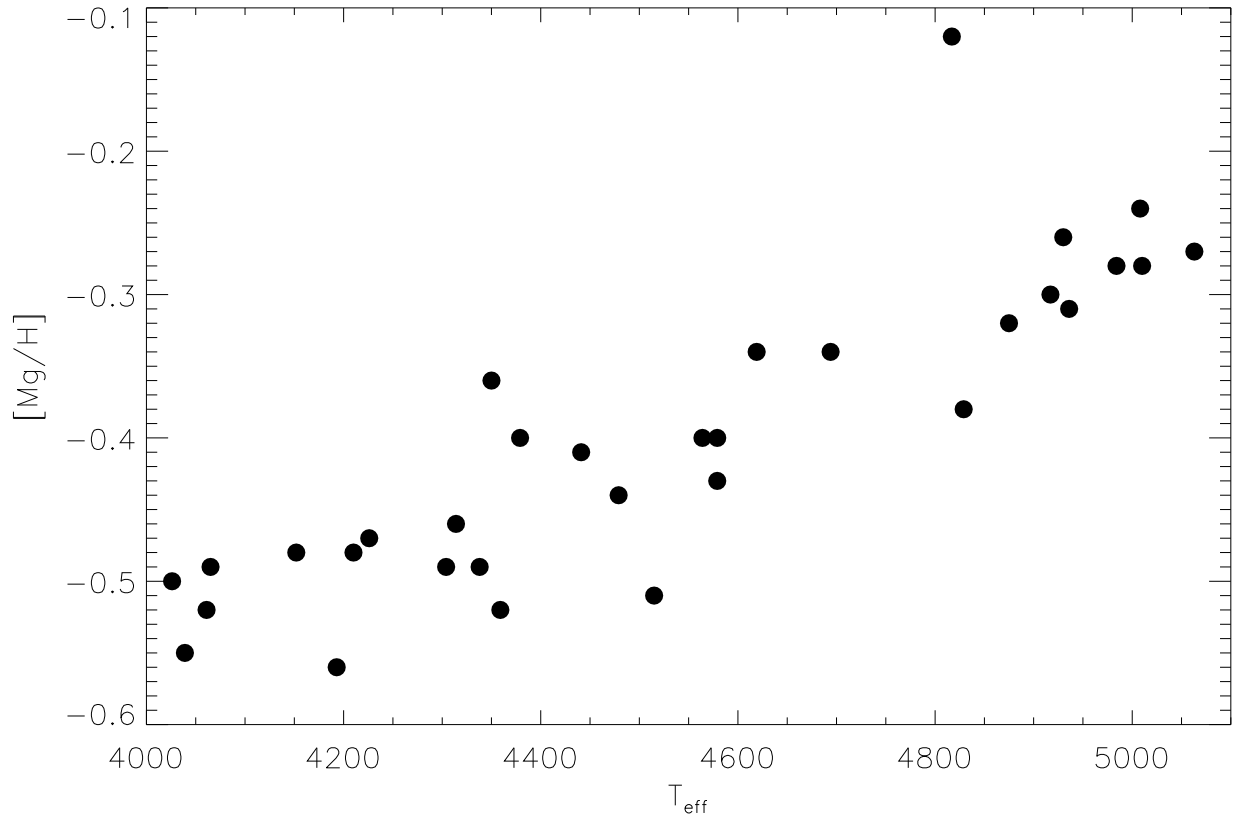


Fig. 11.— Mg abundance (derived from MgH lines) versus T_{eff} . There is a significant trend of $[\text{Mg}/\text{H}]$ with T_{eff} as well as an offset with respect to the Paulson et al. (2003) values. (Paulson et al. derive $[\text{Mg}/\text{Fe}] \simeq 0.0$ which corresponds to $[\text{Mg}/\text{H}] \simeq 0.16$.)

Table 1. Atomic line list

Species	Wavelength (\AA)	χ (eV)	$\log gf$
Fe I	5322.041	2.28	-2.84
Fe I	5811.919	4.14	-2.43
Fe I	5853.161	1.49	-5.28
Fe I	5855.086	4.61	-1.60
Fe I	5856.096	4.30	-1.64
Fe I	5858.785	4.22	-2.26
Fe I	5927.797	4.65	-1.09
Fe I	5933.803	4.64	-2.23
Fe I	5940.997	4.18	-2.15
Fe I	5956.706	0.86	-4.61
Fe I	5969.578	4.28	-2.73
Fe I	6019.364	3.57	-3.36
Fe I	6027.051	4.08	-1.09
Fe I	6054.080	4.37	-2.31
Fe I	6105.130	4.55	-2.05
Fe I	6151.618	2.18	-3.29
Fe I	6157.728	4.08	-1.11
Fe I	6159.380	4.61	-1.97
Fe I	6165.360	4.14	-1.47
Fe I	6173.336	2.22	-2.88
Fe II	4491.407	2.86	-2.49
Fe II	4508.290	2.86	-2.31
Fe II	4620.520	2.83	-3.23
Fe II	5197.559	3.23	-2.25
Fe II	5264.810	3.23	-3.15
Fe II	5325.559	3.22	-3.17
Fe II	5414.046	3.22	-3.62
Fe II	5425.247	3.20	-3.21
Fe II	6149.246	3.89	-2.72

Table 2. The program stars

Name	$B - V^a$	T_{eff} (K)	$\log g$ (cm s^{-2})	ξ_t km s^{-1}	Macro	Region1	Region2 $^{24}\text{Mg};^{25}\text{Mg};^{26}\text{Mg}$	Region3	Final ratio ^b
HIP 20557	0.52	6172	4.42	0.7
HIP 21112	0.54	6084	4.44	0.6
HIP 20237	0.56	6020	4.46	0.6
HIP 19148	0.59	5885	4.49	0.6
HIP 20577	0.60	5846	4.49	0.6
HIP 21317	0.63	5756	4.51	0.6
HIP 19786	0.64	5714	4.52	0.7
HIP 20741	0.66	5652	4.53	0.7
HIP 19793	0.66	5677	4.52	0.7
HIP 20146	0.72	5470	4.56	0.7
HIP 20130	0.75	5393	4.57	0.5
HIP 20480	0.76	5359	4.57	0.6
HIP 23498	0.77	5352	4.58	0.5
HIP 24923	0.77	5334	4.57	0.5
HIP 20949	0.77	5331	4.57	0.6
HIP 21741	0.81	5198	4.59	0.5
HIP 19934	0.81	5215	4.60	0.3
HIP 20951	0.83	5177	4.60	0.6
HIP 22380	0.83	5145	4.61	0.6
HIP 20850	0.84	5127	4.61	0.4
HIP 16529	0.84	5104	4.61	0.4
HIP 13806	0.86	5073	4.61	0.6
HIP 20492	0.86	5101	4.61	0.6
HIP 20978	0.87	5082	4.62	0.4
HD 29159	0.87	5063	4.62	0.6	3.25	77:10:13	75:13:12	80:08:12	77:10:13
HD 28878	0.89	5010	4.63	0.6	3.75	70:16:14	78:11:11	77:09:13	74:13:13
HIP 19098	0.89	4978	4.63	0.4	4.50	77:12:11	81:10:09	81:05:14	79:10:11
HIP 18327	0.90	4984	4.63	0.3	4.25	79:09:12	81:09:10	80:08:12	80:09:11
HIP 16908	0.92	4900	4.64	0.3	1.50	76:11:13	78:10:12	81:07:12	78:10:12
HD 28977	0.92	4936	4.64	0.5	3.75	77:12:11	79:10:11	81:06:13	78:10:12
HIP 13976	0.93	4875	4.65	0.4	2.25	76:12:12	82:05:13	80:08:12	78:09:13
HIP 20827	0.93	4917	4.64	0.4	3.25	74:13:13	78:10:12	78:10:12	77:11:12
HIP 23312	0.96	4799	4.66	0.3	2.25	78:10:12	80:09:11	79:09:14	79:09:12
HIP 20082	0.98	4817	4.66	0.4	1.00	74:13:13	78:09:13	80:09:11	78:10:12
HIP 19263	1.01	4694	4.68	0.3	2.00	75:12:13	77:11:12	79:11:10	76:12:12
HIP 20563	1.05	4619	4.69	0.3	1.25	76:11:13	82:08:10	80:10:10	79:10:11
HIP 18322	1.07	4540	4.69	0.3	1.50	71:15:14	78:11:11	77:12:11	74:13:13
HIP 22654	1.07	4540	4.69	0.3	1.75	75:11:14	77:10:13	76:13:11	76:11:13
HIP 21723	1.07	4534	4.70	0.3	1.25	78:10:12	80:10:10	79:11:10	78:11:11
HIP 18946	1.10	4485	4.70	0.3	1.25	75:12:13	79:10:11	76:13:11	76:12:12
HIP 22253	1.11	4449	4.71	0.3	1.75	77:10:13	81:09:10	79:11:10	79:10:11
HIP 15563	1.13	4411	4.71	0.3	1.50	75:12:13	83:08:09	83:08:09	81:09:10
HIP 20762	1.15	4359	4.73	0.3	1.25	74:12:14	78:11:11	77:12:11	77:11:12
HIP 18018	1.16	4349	4.72	0.3	1.00	77:10:13	83:09:08	82:09:09	80:10:10
HIP 22271	1.17	4320	4.73	0.3	1.00	77:11:12	84:07:09	81:10:09	81:09:10
HIP 19207	1.18	4308	4.73	0.3	1.00	76:11:13	81:09:10	80:11:09	79:10:11
HIP 19441	1.19	4284	4.73	0.3	1.25	78:10:12	83:08:09	83:09:08	81:09:10
HIP 21261	1.20	4274	4.73	0.3	1.00	76:11:13	82:09:09	83:08:09	81:09:10

Table 2—Continued

Name	$B - V^a$	T_{eff} (K)	$\log g$ (cm s^2)	ξ_t km s^{-1}	Macro	Region1	Region2 $^{24}\text{Mg}:^{25}\text{Mg}:^{26}\text{Mg}$	Region3	Final ratio ^b
HIP 19808	1.20	4210	4.75	0.3	1.00	81:09:10	83:07:10	82:10:08	82:09:09
HIP 20485	1.23	4193	4.75	0.3	1.00	74:12:14	78:09:13	79:12:09	77:11:12
HIP 21256	1.24	4196	4.74	0.3	1.25	81:09:10	82:08:10	81:10:09	81:09:10
HIP 22177	1.28	4122	4.75	0.3	1.00	75:10:15	80:10:10	85:07:08	80:09:11
HIP 21138	1.28	4065	4.76	0.3	1.00	80:09:11	77:09:14	81:10:09	80:09:11
HIP 19316	1.33	4031	4.76	0.3	1.00	77:11:12	79:09:12	80:11:09	79:10:11
HIP 17766	1.34	4009	4.77	0.3	1.25	75:11:14	77:10:13	76:14:10	76:12:12
HIP 19082	1.35	3996	4.77	0.3	1.00	78:10:12	80:09:11	81:10:09	80:10:10

^a $B - V$ values taken from Allende Prieto & Lambert (1999)

^bWeighted mean of the ratios derived for regions 1, 2, and 3 weighted by the χ^2 errors

Table 3. Comparison with Paulson et al. (2003) and de Bruijne et al. (2001)

Star	This study		Paulson et al. (2003)		de Bruijne et al. (2001)	
	T_{eff}	$\log g$	T_{eff}	$\log g$	T_{eff}	$\log g$
HIP 20557	6172	4.42	6400	4.3	6275	4.41
HIP 21112	6084	4.44	6250	4.3	6186	4.42
HIP 20237	6020	4.46	6200	4.3	6107	4.44
HIP 19148	5885	4.49	6100	4.5	5983	4.46
HIP 20577	5846	4.49	6050	4.4	5961	4.47
HIP 21317	5756	4.51	5900	4.4	5844	4.49
HIP 19786	5714	4.52	5900	4.4	5812	4.50
HIP 20741	5652	4.53	5800	4.4	5735	4.51
HIP 19793	5677	4.52	5750	4.4	5757	4.51
HIP 20146	5470	4.56	5600	4.5	5553	4.54
HIP 20130	5393	4.57	5550	4.5	5485	4.55
HIP 20480	5359	4.57	5500	4.5	5449	4.55
HIP 23498	5352	4.58	5500	4.5	5429	4.56
HIP 24923	5334	4.57	5500	4.5	5429	4.56
HIP 20949	5331	4.57	5500	4.5	5426	4.56
HIP 21741	5198	4.59	5350	4.5	5303	4.57
HIP 19934	5215	4.60	5350	4.5	5297	4.57
HIP 20951	5177	4.60	5300	4.5	5254	4.58
HIP 22380	5145	4.61	5300	4.6	5249	4.58
HIP 20850	5127	4.61	5350	4.6	5235	4.58
HIP 16529	5104	4.61	5250	4.6	5223	4.58
HIP 13806	5073	4.61	5200	4.6	5196	4.58
HIP 20492	5101	4.61	5200	4.6	5196	4.58
HIP 20978	5082	4.62	5250	4.6	5172	4.58
HD 29159	5063	4.62	5000	4.6
HD 28878	5010	4.63	5150	4.6
HIP 19098	4978	4.63	5150	4.6	5114	4.59
HIP 18327	4984	4.63	5050	4.6	5103	4.59
HIP 16908	4900	4.64	5050	4.6	5054	4.59
HD 28977	4936	4.64	5150	4.6
HIP 13976	4875	4.65	5000	4.6	5034	4.60
HIP 20827	4917	4.64	5050	4.6	5028	4.60
HIP 23312	4799	4.66	5100	4.6	4970	4.60
HIP 20082	4817	4.66	4900	4.6	4924	4.61
HIP 19263	4694	4.68	4874	4.61
HIP 20563	4619	4.69	4785	4.62
HIP 18322	4540	4.69	4749	4.62
HIP 22654	4540	4.69	4749	4.62
HIP 21723	4534	4.70	4744	4.62
HIP 18946	4485	4.70	4703	4.63
HIP 22253	4449	4.71	4672	4.63
HIP 15563	4411	4.71	4640	4.64
HIP 20762	4359	4.73	4611	4.64
HIP 18018	4349	4.72	4586	4.64
HIP 22271	4320	4.73	4560	4.65
HIP 19207	4308	4.73	4550	4.65
HIP 19441	4284	4.73	4527	4.65
HIP 21261	4274	4.73	4515	4.65

Table 3—Continued

Star	This study		Paulson et al. (2003)		de Bruijne et al. (2001)	
	T_{eff}	$\log g$	T_{eff}	$\log g$	T_{eff}	$\log g$
HIP 19808	4210	4.75	4500	4.65
HIP 20485	4193	4.75	4438	4.66
HIP 21256	4196	4.74	4425	4.66
HIP 22177	4122	4.75	4320	4.66
HIP 21138	4065	4.76	4312	4.66
HIP 19316	4031	4.76	4129	4.67
HIP 17766	4009	4.77	3980	4.71
HIP 19082	3996	4.77	3944	4.72

Table 4. Abundance dependences on model parameters

Star	Model parameter	$\log\epsilon(\text{Fe I})$	$\log\epsilon(\text{Fe II})$
HIP 20557 ($T_{\text{eff}}=6172$)	$T_{\text{eff}} + 100\text{K}$	0.06	-0.01
	$\log g - 0.2 \text{ dex}$	0.01	-0.04
	$\xi + 0.2 \text{ km s}^{-1}$	-0.03	-0.07
HIP 20146 ($T_{\text{eff}}=5470$)	$T_{\text{eff}} + 100\text{K}$	0.07	-0.04
	$\log g - 0.2 \text{ dex}$	0.00	-0.06
	$\xi + 0.2 \text{ km s}^{-1}$	-0.03	-0.06
HIP 19098 ($T_{\text{eff}}=4978$)	$T_{\text{eff}} + 100\text{K}$	0.02	-0.08
	$\log g - 0.2 \text{ dex}$	-0.01	-0.09
	$\xi + 0.2 \text{ km s}^{-1}$	-0.02	-0.03
HIP 18946 ($T_{\text{eff}}=4485$)	$T_{\text{eff}} + 100\text{K}$	-0.01	-0.14
	$\log g - 0.2 \text{ dex}$	-0.02	-0.13
	$\xi + 0.2 \text{ km s}^{-1}$	-0.01	-0.02
HIP 19082 ($T_{\text{eff}}=3996$)	$T_{\text{eff}} + 100\text{K}$	-0.08	-0.29
	$\log g - 0.2 \text{ dex}$	-0.07	-0.21
	$\xi + 0.2 \text{ km s}^{-1}$	-0.01	-0.01